MODELING SECONDARY EMISSION IN A FINITE-ELEMENT MULTIPACTOR CODE[*]

S. Humphries[+], Department of Electrical and Computer Engineering, University of New Mexico, Albuquerque, NM 87131 USA, J. Petillo, SAIC, Burlington, MA 01803 USA, and N. Dionne, Raytheon Corporation, Sudbury, MA 01776 USA.

Abstract

Accurate calculations of secondary emission processes are important to model multipactacting in RF devices. The angular dependence of δ (the secondary-emission coefficient) and the direction of ejected secondary electrons requires a knowledge of the material surface orientation at the collision point. We describe methods to find normal vectors on arbitrary surfaces represented by conformal triangular meshes. The information is applied to secondary emission calculations in the Trak_RF code. Discussions cover expressions for the energy and angular dependencies of δ, procedures to assign kinetic energy and initial directions to secondary electrons, and particle accounting in simulations that may follow several generations. The methods are illustrated with benchmark simulations of multipacting in a superconducting accelerator cavity. This application, involving small-scale orbits confined near the cavity wall, illustrates the advantages of a conformal mesh. Furthermore, the example shows that detailed emission models significantly affect electron histories and are essential to achieve agreement with experiments.

1. INTRODUCTION

Models of secondary electron emission from surfaces are often important in charged-particle simulations of high-power devices[1-9]. Examples include estimation of the efficiency of multi-stage collectors in vacuum tubes[10] and multipacting in RF feeds and accelerator cavities[11,12]. The validity of the calculations may depend on accurate representations of the variation of the secondary emission coefficient δ with incident particle angle and the distributions of emitted electrons in energy and direction. The quantity δ equals the number of electrons emitted per incident electron. Calculation of these quantities requires a knowledge of the local orientation of emission surfaces. Routines to find the surface vectors must function reliably with complex system geometries.
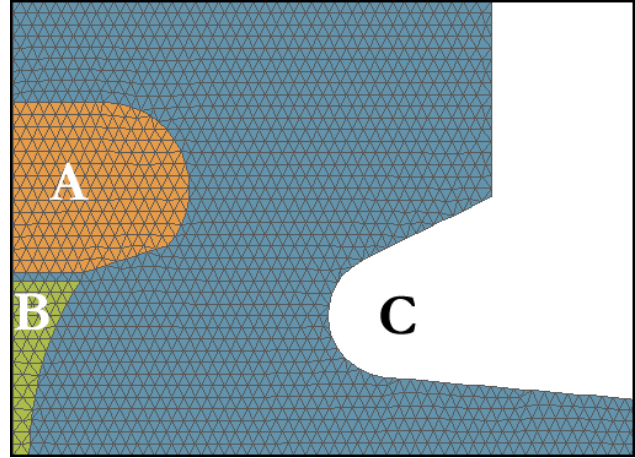
+ E Mail: humphrie@eece.unm.edu

Figure 1. Conformal mesh for an electron gun.

This paper describes a direct geometric method to find surface normal vectors in two-dimensional systems represented by a triangular mesh[13]. This information can be used to correct the secondary emission coefficient for angle and to generate realistic distributions of emitted electrons. The procedures are illustrated with benchmark multipactor calculations using the Trak_RF code[14]. Topics covered include organization of the code to identify elements associated with different emitting materials and expressions for the unit vector of arbitrary surfaces in planar and cylindrical systems. The benchmark simulation applies to a superconducting cavity[11] tested at Stanford University. Detailed experimental and theoretical results are available for comparison. The calculation illustrates the importance of detailed emission models for agreement with experiments. Even though peak field levels in the cavity are in the range 10 MV/m, emission energies of 2 eV can significantly affect the nature of the solution.

2. FINITE-ELEMENT MULTIPACTOR CODE ORGANIZATION

The element viewpoint for the generation of electromagnetic difference equations is based on the division of a solution volume into small segments with unique material indentities[13,15-17]. Ideally, the boundaries of elements should closely follow the boundaries of physical objects in the system. In this case difference solutions can yield accurate field values along complex surfaces. This paper concentrates on systems with two-dimensional symmetry where the geometry is represented by projections in either the

x-y or *r-z* planes. Areas in the planes are divided into small triangles. In planar simulations the set of volume elements consists of bars with triangular cross-section that extend a unit distance in *z*. The elements in cylindrical calculations are toroidal figures of revolution about the axis. In a *conformal* triangular mesh, the sides of the elements are shifted so that vertices lie along material surfaces. Figure 1 shows an example of a conformal mesh for an electron gun. The advantage is apparent. The element boundary segments closely follow the curved surfaces of electrodes.

In the Trak_RF program a *region* is defined as a set of contiguous elements with the same material identity. For example, the elements that represent the focus electrode of the electron gun of Fig. 1 (marked *A*) have fixed electrostatic potential. The vacuum (corresponding to the outlined elements) is a region of complex shape with relative dielectric constant $\epsilon_r = 1$. Elements are assigned identifying region numbers during mesh generation. Vertices also have region numbers. These numbers may be the same as those of the surrounding elements. Sometimes, vertices have unique region numbers to mark special surfaces like the emitting face of the cathode (*B*). Regions in Trak_RF are divided into three types: *vacuum*, *material* and *secondary*. Particles in *vacuum* regions propagate under the influence of the calculated electric and magnetic fields. An electron is absorbed when it enters a *material* element. In this case, the program terminates the orbit and records the final parameters. When an electron enters a *secondary* material it is restarted at the entrance position. The current, kinetic energy and emission direction of the secondary are determined by the properties of the incident electron. The Trak_RF program can include information for electromagnetic, electrostatic and magnetostatic fields on independent conformal meshes. Material characteristics can be associated with regions on any of the three meshes. The program responds to the detection of *material* or *secondary* elements on any of the meshes in the following order of precedence: electromagnetic, magnetic and then electrostatic.

There are several options in electron orbit codes to represent the creation of new particles through secondary emission. To make optimal use of storage arrays Trak_RF employs a constant number of independent computational particles. An individual computational particle represents a possible history that may include several generations of secondaries. In each wall collision the current carried by the particle is adjusted by a factor equal to secondary emission coefficient δ. It is possible to introduce statistical variations by starting multiple primary electrons from each initiation point.
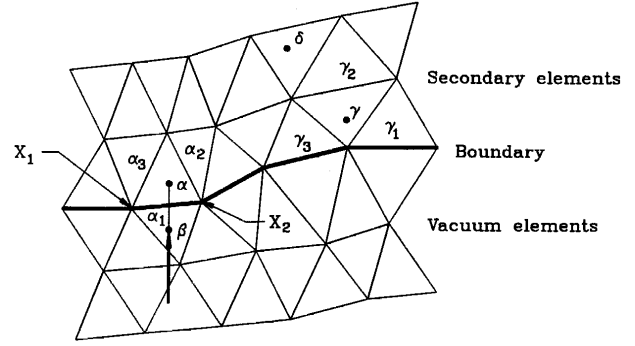

Figure 2. Elements near the surface of a secondary material

3. SURFACE NORMAL VECTORS

During an orbit integration Trak_RF determines the element region number at the particle position at each time step as part of the field interpolation process. The program then checks a status array to see if the region is a secondary material. In this case the program seeks a surface normal vector. Figure 2 shows an event where a particle enters a secondary element adjacent to a vacuum. The point marked α is the current position and β is the position at the previous time step before entering the secondary element. The figure also shows the known momentum vector at point β. In this case the procedure to find the surface normal is straightforward. The program checks the material identity of the three elements marked α_1, α_2 and α_3 adjacent to the sides of the target triangle. It picks the side of the target triangle that is adjacent to a vacuum element. If there is more than one such side, the program chooses the one closest to point α. The end points of the side are designated as the vectors $\mathbf{X}_1$ and $\mathbf{X}_2$, ordered in the sense of positive rotation. For a planar field simulation (with variations in the x-y plane and infinite extent in z) the vectors are $\mathbf{X}_1 = (x_1, y_1, 0)$ and $\mathbf{X}_2 = (x_2, y_2, 0)$. The unit vector pointing out of the surface of the secondary element into vacuum is $(\mathbf{X}_2 - \mathbf{X}_1) \times \mathbf{z}$, or

$$u_n = \frac{(y_2 - y_1)\ x - (x_2 - x_1)\ y}{\sqrt{(x_2 - x_1)^2 + (y_2 - y_1)^2}} . \qquad (1)$$

Orbit integrations in Trak_RF are performed in three-dimensional Cartesian coordinates for fields with both planar and cylindrical symmetry. Therefore, the three momentum components are known at all times. The momentum components at point β can be used to approximate a unit vector aligned along the incident trajectory,

$$u_p = \frac{p_x\ x + p_y\ y + p_z\ z}{\sqrt{p_x^2 + p_y^2 + p_z^2}} . \qquad (2)$$

The incident angle θ of particle relative to surface is defined as angle between the surface normal and the negative of the

incident particle vector. For this convention normal incidence corresponds to $\theta = 0°$ and grazing incidence is $\theta = 90°$. The angle can be determined from the dot product of the unit vectors,

$$\cos\theta = -\boldsymbol{u_n}\cdot\boldsymbol{u_p} \; , \qquad (3)$$

or

$$\cos\theta = \frac{p_y(x_2-x_1) - p_x(y_2-y_1)}{\sqrt{p_x^2+p_y^2+p_z^2}\;\sqrt{(x_2-x_1)^2+(y_2-y_1)^2}} \qquad (4)$$

For cylindrical symmetry, the mesh coordinates give unit vector components along r and z,

$$\boldsymbol{u_n} = u_r\boldsymbol{r} + u_z\boldsymbol{z} = \frac{-(z_2-z_1)\,\boldsymbol{r} + (r_2-r_1)\,\boldsymbol{z}}{\sqrt{(z_2-z_1)^2+(r_2-r_1)^2}} \; . \qquad (5)$$

If the electron position at the secondary surface is (x,y,z), then the surface normal vector in Cartesian coordinates is

$$\boldsymbol{u_n} = u_r\cos\alpha\;\boldsymbol{x} + u_r\sin\alpha\;\boldsymbol{y} + u_z\;\boldsymbol{z} \; . \qquad (6)$$

where $\alpha = \tan^{-1}(y/x)$. Taking the dot product of the vector defined by Eq. 5 or 6 with $-\boldsymbol{u}_p$ gives the relative incidence angle.

An exceptional case occurs when an electron enters a secondary element of the type marked γ in Fig. 2. This element is adjacent to the boundary but has no side that borders a vacuum. For this situation the program checks the three adjacent triangles γ_1, γ_2 and γ_3. If the triangle corresponds to a secondary, the program looks for a vacuum boundary and uses the corresponding side as the surface of the material. If there are several vacuum sides, the program picks the one closest to point γ. If no vacuum boundary is located after this procedure, it means that the electron is buried deeply in the material (point δ in Fig. 2). This condition may occur if the time step is too long, allowing the electron to cross more than one cell per step. In this case, the program issues a warning and terminates the orbit.

4. SECONDARY EMISSION MODELS

Trak_RF determines the secondary emission coefficient from a parametric model based on work by Jonker[18] and Vaughn[19]. Conveniently the model involves the cosine of the incident electron angle given by Eq. 4. The defining function for the angular dependence of δ is

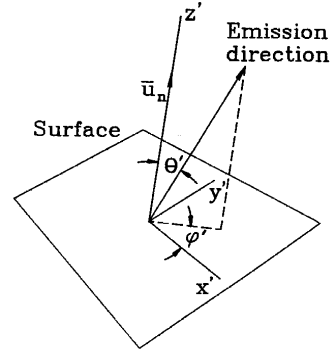$$F(\theta) = \frac{1}{\sqrt{\cos(\theta)}} \; . \qquad (7)$$

Figure 3. Emission directions

The maximum value of secondary coefficient and the corresponding incident electron energy are given by

$$\delta_m = \delta_{mo}\,F(\theta),$$
$$E_m = E_{mo}\,F(\theta), \qquad (8)$$

where δ_{mo} and E_{mo} are the values at normal incidence. These quantities are tabulated for a variety of materials in Ref 20. The secondary emission coefficient as a function of the angle θ and kinetic energy E of the incident electron is given approximately as

$$\delta(\theta,E) = \delta_m\left[\,f\,e^{(1-f)}\,\right]^a \; , \qquad (9)$$

where $f = E/E_m$. The parameter a has the value 0.62 for $f < 1$ and 0.25 for $f \geq 1$. Trak_RF stores parameters for up to ten different secondary emission materials in a run. Any number of secondary regions can be associated with a secondary material. In defining materials, the user has the option to add enhancement factors ζ to represent the effects of surface imperfections. The program multiples calculated values of δ by the value of ζ for the material. It is also possible to turn off angular corrections and re-emission parameters to gauge the effect of the model. In this case, secondary electrons are created at the entrance (point β in Fig. 2) with zero kinetic energy.

We next consider emission models. Following Ref. 21, the program creates secondary electrons with the Maxwell distribution,

$$n(E) \sim E^{\frac{1}{2}}\exp\left(-\frac{E}{2E_p}\right) , \qquad (10)$$

where $E_p = 2.0$ eV.

The program determines the total momentum p_o from the kinetic energy and then assigns momentum components based on the emission direction. In the absence of detailed information, the program assumes uniform probability over the solid angle pointing from the surface into the vacuum. If the quantities θ' and ϕ' are the polar angles about the surface normal (Fig. 3), then the normalized probability distribution for emission over $0 \leq \theta' \leq \pi/2$ is

$$p(\theta', \phi') = \frac{\sin\theta}{2\pi} . \qquad (11)$$

To make a weighted normalized distribution, the program generates two random values in range $0 \leq \chi_1, \chi_2 \leq 1$ and computes the polar angles according to,

$$\phi' = 2\pi\chi_1,$$
$$\theta' = \sin^{-1}(\chi_2). \qquad (12)$$

The polar angles can be used to find the momentum components in the (x',y',z') coordinate system of Fig. 3 where the z' axis is aligned along surface normal,

$$p'_x = p_o \sin\theta' \cos\phi',$$
$$p'_y = p_o \sin\theta' \sin\phi', \qquad (13)$$
$$p'_z = p_o \cos\theta'.$$

The quantities of Eq. 13 can then be transformed to the actual coordinates of the simulation. In planar simulations we assume that x'-z' is coplanar with x-y. If the quantity α is the angle between the z' and x axes., then the transformation is given by,

$$p_z = p'_y,$$
$$p_x = p'_z \cos\alpha - p'_x \sin\alpha, \qquad (14)$$
$$p_y = p'_z \sin\alpha + p'_x \cos\alpha.$$

A similar transformation holds for cylindrical systems.

5. BENCHMARK CALCULATION

We shall illustrate the implementation of the secondary models with benchmark simulations of single-point multipacting in a superconducting resonant cavity investigated at Stanford University[11]. Published experimental data and previous numerical simulations are
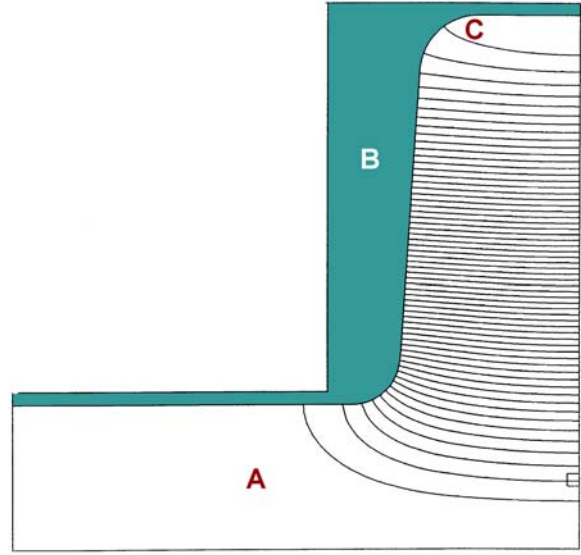

Figure 4. Half of cavity for benchmark simulation

available for comparisons. In contrast to the previous work, the code described in this paper can be applied to a wide variety of RF devices. The single-point multipactor process has the following mechanism. It starts when a stray electron is accelerated away from the cavity surface by the RF electric fields. Under some circumstances the particle may return to a point near the original at about the same RF phase. The number of electromagnetic periods that elapse between the generation and return of an electron is called the *order* of multipactor. If the kinetic energy of the returning electron is in a range to give $\delta > 1$, then additional electrons may leave the surface. The process may generate a growing electron density. The flow of current represents an energy loss in superconducting cavities and may lead to local heating or breakdown. These processes are possible even at low electron densities where the electric field generated by space-charge is small compared to the RF electric field. Therefore, it is sufficient to track electron orbits individually in the applied RF field.

Figure 4 illustrates the simulation geometry for half of the cavity (utilizing a symmetry boundary at the midplane). Electric field lines for the TM_{010} mode are included. Reference 11 shows that conditions for multipacting (phase synchronization and the correct kinetic energy range for returning electrons) are satisfied only on the outer wall near the point of transition from curved to flat surface (point *C*). Here the small radial component of electric field moves electrons away from the wall. They return to nearby locations after following complex orbits in the combined electric and magnetic fields of the RF mode. The challenge of this calculation is to solve for the global electromagnetic fields while maintaining sufficient accuracy near the wall to follow electron orbits with excursions less than 1 mm. In this application the conformal, variable-resolution mesh of Trak_RF offers an advantage. The mesh used had moderate resolution over most of the cavity volume to reduce run time and fine resolution near the outer wall for high-accuracy field

interpolations.

The resonant frequency (2.8 GHz) and fields of the TM_{010} mode were determined with the WaveSim program[22]. The solution file was ported to Trak_RF for orbit tracking. Values in the file could be multiplied by a normalization factor to check different values of field amplitude. For comparison to Ref. 11 the maximum on-axis cavity field, $E_z(0,0)$, is used to parametrize runs. The assignment of regions is simple. All elements inside the cavity (*A*) have vacuum properties, and all elements of the wall (*B*) correspond to a secondary material with the properties of niobium. In the WaveSim calculation the wall elements have the properties of an ideal void[12] which enforces a Neumann boundary condition on rH_θ. After loading and normalizing field information, the next step in a Trak_RF solution is specification of the initial positions, directions and phase (with respect to the RF field) of up to 2000 particles. For the multipactor simulations electrons were created with zero kinetic energy in the vacuum region close to the outer wall. Orbits were followed for 50 ns (150 RF periods). Each orbit had an initial weight of 1.0 that was multiplied by δ on each collision. Multipacting could occur for particles that had a final weighting factor much larger than unity and that did not move a substantial distance along the wall. The program also counted the total number of wall strikes in a run to determine if the synchronization conditions were satisfied. Orbits were terminated if they left the system or exceeded the maximum run time. It was necessary to include additional stopping criteria in Trak_RF to ensure that wall strikes were not dominated by spurious electron interactions. Orbits were stopped under the following conditions:

> 1) The kinetic energy of electrons impacting the wall fell below a cutoff value. With this condition the program avoids counting electrons with very low energy (a few eV) that sometimes could be trapped near the cavity midplane.
> 2) The electron was in secondary element on the previous time step. This condition indicates that the wall interaction has occurred in the decelerating phase of the RF field.
> 3) The relative current fells below a minimum value (10^{-4}). This condition may occur for electrons that oscillate near the wall at low kinetic energy.

Initial runs were performed with electron emission over an extended area covering the wall of the cavity. These studies confirmed that orbit synchronization and the correct kinetic energy range occurred only in the region near point *C* of Fig. 4. For electron emission from this region it was possible to achieve multiplying orbits in field amplitude bands in the phase range

$$0° \leq \Delta\phi \leq 110°. \qquad (15)$$

Here, the electric field at the initial point varied as $E_r \sim \sin(2\pi ft)$ and $E_z \sim -\sin(2\pi ft)$. Figure 5 shows the number of wall strikes as a function of $E_z(0,0)$ for electrons emitted at point *C* of Fig. 5 in 10° phase intervals over the range of Eq.
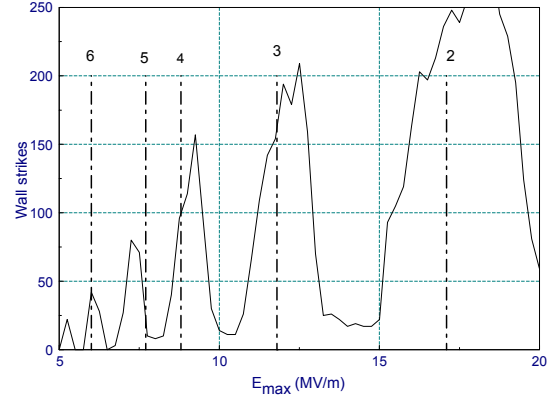

Figure 5. Number of wall strikes in the benchmark simulation

15. There are clearly-defined bands of electron multiplication. The numbers near the bands show the multipactor order determined from a list of wall strike times created by the code. The amplitude difference between bands is not highly significant. It reflects that fact that more collisions are possible in the lower order bands over the integration time of 50 ns. The dashed line shows measured field values from Ref. 11 for local cavity heating on the outer wall. The simulations show good absolute agreement with the experiments and are in almost exact agreement with previous simulations[11].

Electron orbit plots provide a clear demonstration of the importance of the detailed emission models. Figure 6 shows *r-z* projections of the orbits of electrons emitted from point *C* of Fig. 4 with a phase of 30°. The field amplitude $E_z(0,0)$ = 12.2 MV/m corresponds to the third-order multipactor band. The outer wall is at the top of the plot. Figure 6*a* shows results with a simplified emission model where secondary electrons are created with zero kinetic energy at the point of impact. In this case motion is limited to a single *r-z* plane because the electric and magnetic forces of the TM_{010} mode exert no azimuthal force. The electron follows an orderly motion. The maximum impact kinetic energy occurs near the initiation point and the maximum displacement from the wall is less than 1 mm. The electron follows an orderly drift toward the cavity midplane with steadily decreasing impact kinetic energy. The orbit of Fig. 7*a* is not consistent with multipacting. All orbits have relatively low kinetic energy and drift to the cavity midplane after only a few wall strikes. The situation changes dramatically with detailed emission models (Fig. 7*b*). Even though the peak cavity fields are large (10 MV/m), the small emission energy (~2 eV) substantially affects the small-scale particle orbits near the wall. They exhibit larger excursions,
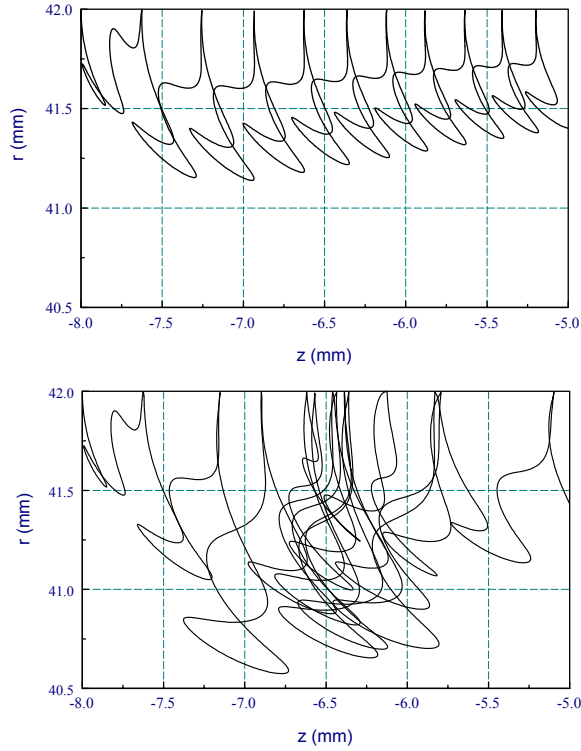
Figure 7. Global multiplication factor for the benchmark simulation.

Figure 6. Electron orbits at the cavity outer wall. Top: Zero energy emission. Bottom: Detailed emission model.

increased impact kinetic energy and significant azimuthal motion. Including a random emission direction creates classes of electrons that evolve through many generations near the point of maximum kinetic energy. In this case it is possible to build up a substantial electron density before the ultimate drift to the midplane. The orbit of Fig 6*b* is almost identical to those illustrated in Ref. 11.

Finally, Fig. 7 shows a plot of the global multiplication factor as a function of field amplitude for the full emission model. Again, electrons are emitted from point *C* of Fig. 5 over the phase range of Eq. 15. In the plot a value of unity indicates that all electrons returned in the wrong phase of RF field on the first strike and were lost. (The final number of electrons equals the initial number.) Values less than unity indicate that there were multiple strikes but the electrons returned in a kinetic energy range such that $\delta < 1$. Finally, values much larger than unity illustrate the possibility of true multipactor with the effects of impact energy, synchronization and electron drift included. In agreement with Ref. 11, the Trak_RF program showed that multipactor did not occur at any field level for walls with the secondary emission coefficient of pure niobium. A value of the enhancement factor ζ greater than unity was necessary to achieve multiplication factors higher than unity. The values of Figure 7 correspond to $\zeta = 2.0$. Electron growth occurs in the second and third order bands. Increased values of ζ lead to multiplication in higher order bands. These results are in agreement with those of Ref. 11
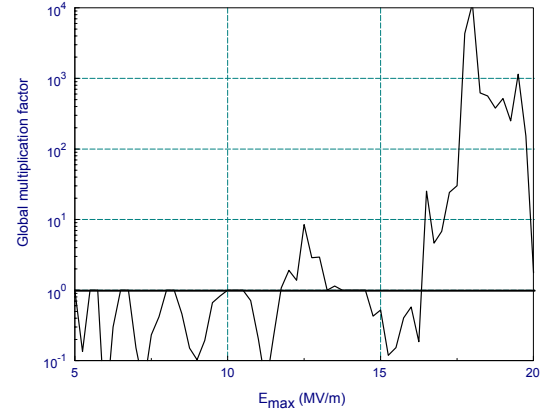
considering that the multiplication values are extremely sensitive to the value of ζ and the choice of initial orbits.

In conclusion, the finite-element Trak_RF code incorporates secondary emission models based on the direct determination of the local orientation of emitting surfaces. The model is robust. The multipactor simulations covered thousands of wall strikes without a program error. The secondary emission models had little effect on the run time of the code because the time step is generally chosen so that electrons move over less than a single element in a step. Furthermore, the operations to find the orientation of local surfaces are quick because the target element has been identified by the previous field interpolation. The benchmark calculation illustrates that realistic emission models may significantly influence results in some simulation.

REFERENCES

1. See, for instance, S. Humphries, Jr., **Charged Particle Beams** (Wiley, New York, 1990), Sect. 7.3.
2. N.J. Dionne and H.J. Krahn (Raytheon Company, PT5599, 1980), unpublished.
3. W.B. Herrmannsfeldt (Stanford Linear Accelerator Center, SLAC-331, 1988), unpublished.
4. A.C. Paul (Lawrence Berkeley Laboratory, LBL-13241, 1982), unpublished.
5. D.L. Vogel (Lawrence Berkeley Laboratory, LBL-18871, 1985), unpublished.
6. J.E. Boers (Sandia National Laboratory, SAND 79-1027, 1980), unpublished.
7. R. True, IEEE Trans. Nucl. Sci. **NS-32**, 2611 (1985).
8. R. True, *General Purpose Relativistic Beam Dynamics Code* in **Computational Accelerator Physics**, edited by R. Ryne (Am. Inst. of Physics, New York, 1994), 493.
9. S. Humphries, Jr., J. Comp. Physics **125**, 488 (1996).
10. J.A. Dayton, H.G. Kosmahl, P. Ramins and N. Stankiewicz, IEEE Trans. Electron Devices **ED-26**, 1589 (1979) and IEEE Trans. Electron Devices **ED-28**, 1480 (1981).

11. C.M. Lyneis, H.A. Schwettman and P. Turneaure, Appl. Phys. Lett. **31**, 541 (1977).

12. S. Humphries, Jr., *Electron multipactor code for high-power RF window development*, Particle Accelerators **62**, 139 (1999).

13. See, for instance, S. Humphries, Jr., **Field Solutions on Computers** (CRC Press, Boca Raton, 1997).

14. S. Humphries, Jr. and D. Rees, *Trak_RF - Simulation of electromagnetic fields and particle trajectories in high-power RF Devices*, in E.C. Michielssen (*ed*.), **Proc. Applied Computational Electromagnetics** (Naval Postgraduate School, Monterrey, 1997), 1102.

15. P.E. Allaire, **Basics of the Finite-element Method** (Wm. C. Brown, Dubuque IA, 1985).

16. M.N.O. Sadiku, **Numerical Techniques in Electromagnetics** (CRC Press, Boca Raton, 1992), Chap 6.

17. M.V. Chari and P.P. Silvester, eds., **Finite Elements for Electrical and Magnetic Field Problems** (Wiley, New York, 1980).

18. J.L.H. Jonker, Phillips Research Reports **6**, 372 (1951), Phillips Research Reports **7**, 1 (1952), Phillips Research Reports **12**, 249 (1957).

19. R.M. Vaughn, IEEE Trans. Electron Devices **ED-36**, 1963 (1989) and IEEE. Trans. Electron Devices **ED-40**, 830 (1993).

20. D.R. Lide, ed., **Handbook of Chemistry and Physics, 74th Edition** (CRC Press, Boca Raton, 1993), 12-107

21. R. Kollath, Ann. Physik **6**, 357 (1947).

22. S. Humphries, Jr., *Finite-element solutions for electromagnetic scattering in inhomogenous volumes*, to be published, J. Modern Optics.